



Molecular dynamics simulation of water purification using zeolite MFI nanosheets



Seyed Moein Rassoulinejad-Mousavi^{a,1}, Jafar Azamat^{b,1}, Alireza Khataee^{c,d,*}, Yuwen Zhang^{a,*}

^a Department of Mechanical and Aerospace Engineering, University of Missouri, Columbia, MO, 65211, USA

^b Department of Basic Sciences, Farhangian University, Tehran, Iran

^c Research Laboratory of Advanced Water and Wastewater Treatment Processes, Department of Applied Chemistry, Faculty of Chemistry, University of Tabriz, 51666-16471 Tabriz, Iran

^d Institute of Research and Development, Duy Tan University, Da Nang 550000, Vietnam

ARTICLE INFO

Keywords:

Zeolite nanosheet
Water purification
Mercury chloride
Copper chloride

ABSTRACT

Water purification and detoxification is an important topic that protects the environment and ecosystems. The feasibility of using Zeolite MFI as a nanostructured membrane to remove hazardous chemicals from a contaminated water solution is studied in this paper. A non-equilibrium molecular dynamics analysis was performed to see the potentials of the zeolite porous nanosheet to separate the mercury chloride (HgCl_2) and copper chloride (CuCl_2) from water as two major hazardous contaminants. A reverse osmosis system was simulated and tested at different induced pressures from 10 to 200 MPa. Ion removal, water flux, water molecules accumulation at different locations, number of hydrogen bonds, Van der Waals interactions, ions tracking path and radial distribution function between water molecules and the ions, were investigated in detail. The results indicated that the zeolite MFI nanomembrane can effectively prevent mercury, copper and chlorine ions from permeation while keeping a large water flux through the membrane. This behavior of the zeolite introduces a competitive candidate for the water purification industry and sets it apart from other nanostructured membranes.

1. Introduction

Improving health and lowering carbon footprint are two leading reasons that make water purification a priority. The presence of chemicals and other toxic materials in water sources can cause a broad range of health issues including higher risk of cancer and birth defects. Therefore, it is very important to find a way to keep these impurities out from water. Among the chemicals, copper chloride (CuCl_2) is one of the hazardous chemicals that is on the Special Health Hazardous Substances (SHHS) list and can damage the liver, kidneys, nose, irritating the stomach, throat and lung, burn the skin and eyes with possible eye damage [1]. Another hazardous chemical in water that affects human when inhaled and maybe absorbed through the skin is mercury chloride (HgCl_2). This hazardous chemical, which is also on the SHHS list, is known as very toxic to aquatic life with long-lasting effects [2]. It can irritate the skin and eyes upon exposure and may cause reproductive damage. Repeated exposure can damage organs, cause

cancer and can be fatal.

Recently, the use of nanomembranes has attracted many researchers for water desalination and water treatment. Applications of these types of nanostructured materials have been investigated in reverse osmosis systems (RO) since they are known as more energy-efficient and environmentally friendly among the existing commercial purification techniques [3]. The main reason for their popularity comes from the two main drawbacks of the current RO membranes: low water permeability and membrane fouling [4–6]. Until now, different nanosheet materials including graphene [7], graphene oxide [8], molybdenum disulfide (MoS_2) [9], Boron nitride (BN) [10], silicon carbide [11], and zeolite [12] have been proposed theoretically using atomistic simulations for water desalination, and the nanostructure membranes could efficiently reject salt from water.

The idea of heavy metal removal from water using nanomembranes has been brought to the notice by Azamat et al. [13] using density functional theory, they obtained the optimized graphene structure to

* Corresponding authors at: Research Laboratory of Advanced Water and Wastewater Treatment Processes, Department of Applied Chemistry, Faculty of Chemistry, University of Tabriz, 51666-16471 Tabriz, Iran (A. Khataee). Department of Mechanical and Aerospace Engineering, University of Missouri, Columbia, MO 65211, USA (Y. Zhang).

E-mail addresses: a.khataee@tabrizu.ac.ir (A. Khataee), zhangyu@missouri.edu (Y. Zhang).

¹ SMR and JA contributed equally.

remove copper and mercury from an aqueous solution. On the other strike, they studied the separation of chlorination disinfection by-products from water using functionalized graphene by induced pressure [14]. They recommended small pore sizes in the functionalized graphene for better filtration. Recently, functionalized graphene oxide nanosheets were applied to separate perchlorates from aqueous solution [15].

Separation of zinc ion (Zn^{2+}) from water using two functionalized BN and graphene sheets has been studied by Azamat et al. [16] and their results showed that pore structure plays an important role in number of ions permeation. They also found that barrier energy of Zn^{2+} ions in the BN nanosheet was less than that of graphene. Using potential of mean force, modified BN membranes for carbon dioxide and nitrogen separation were provided [17]. It was shown that, separation occurs only in high energy barrier difference between the two types of molecules.

MoS_2 was used for water detoxification by separation of ions such as mercury [18] and arsenic [19] from contaminated water. It was found that MoS_2 could effectively prevent the penetration of mercury and arsenic due to a higher energy barrier for the ions than water molecules in MoS_2 . They showed that pore structure also had an important role in the separation performance. This has led water molecules to permeate easily through the porous membrane while arsenic and mercury ions were not able to pass through.

However, there is still a long way to go before realistic large-scale fresh water desalination and purification using membranes and needs more research and feasibility study. It is due to the fact that, these systems need to be designed so that they are multifunctional and long-term stable, cost-effective synthesis, with exceptional antifouling, adsorptive, antimicrobial properties [20]. Among membranes recommended in the literature, zeolite MFI has shown a great potential for water desalination with large water fluxes while maintaining high salt rejection [12]. They have perpendicular pores, which enable transport in all dimensions through the crystal [21], and are among the most abundant mineral components on earth [22]. In addition, being the second most important and profitable framework from the standpoint of catalysis and industrial use, and the more general conceived approach which allows extension to other frameworks, make two-dimensional form of zeolite MFI notable [23]. In addition, zeolite has been used for decades as the most privileged fundamental material in wastewater purification and detoxification processes [24].

It is necessary to consider the potential of the zeolite nanosheet for other hazardous ions separation from aqueous especially when they are smaller than Na^+ . However, size is not the only criteria for separation effectiveness of a membrane and other factors are important too, e.g., the density of charge. The ions that were considered in this work (Cu^{2+} and Hg^{2+}) have two positive electric charges which have a different structure than those ions with only one positive electric charge such as Na^+ . On the other hand, Cu^{2+} and Hg^{2+} have a smaller and equal size with respect to Na^+ based on their ionic radius (The ionic radius of $Cu^{2+} = 73$ pm, $Hg^{2+} = 102$ pm and $Na^+ = 102$ pm), respectively; thus, their separation is much more difficult than Na^+ . This work aims to study the capability of zeolite MFI nanosheet in removing mercury chloride and copper chloride as two major contaminants from water. Non-equilibrium molecular dynamics (MD) simulations investigate ions transportation at various applied pressures to consider the water flux and ions separation capability along with other factors.

2. Computational details

The heavy metal ions rejection process from the aqueous solution will be simulated by zeolite MFI nanosheet membrane using the following procedure. A simulation box containing the membrane with a thickness of 20 \AA placed in the center of the box for reverse osmosis separation was designed. An electrically neutral mixture of $HgCl_2$, $CuCl_2$ solution (with 31 Cu^{2+} , 31 Hg^{2+} and 124 Cl^- ions) along with

3200 water molecules were added to one side of the zeolite nanomembrane in the simulation box. Due to the computational cost, the concentration of heavy metals was higher than those in real wastewater. The atomistic structure of zeolite was taken from the IZA database [25] and dangling bonds of silicon atoms of zeolite were saturated with $-OH$ groups.

The dimension of the simulation cell was $38(x) \times 38(y) \times 200(z) \text{ \AA}^3$. The CHARMM force field was used in current simulations, which is compatible with the NAMD package. The implemented force fields in our simulations were chosen to be fully compatible between the zeolite membrane, water molecules, and ions. The force fields parameters for heavy metals were obtained from Azamat et al. [26] and those for the zeolite membrane were taken from Emami et al. [27], which have been previously validated against experimental data. This force field has been applied to study zeolites with a wide range of hydroxyl group densities (the SiOH density on the surface of a zeolite) and pHs. As this force field only considers bond stretching and bond angle bending of the silanol groups on the surface, it is less computationally intensive compared to other proposed force fields such as [28] and [29].

For the water molecules, the various models were all reported in the scientific literature. It is worth to note that choice of these force fields may affect the simulation results, but currently no consensus has been reached on the most appropriate force field for simulating the zeolite-based water purification membranes. However in this work, the TIP3P [30] water model was used due to its success in modeling water [31,32] including zeolite-water [12]. Non-equilibrium MD simulations were performed by the NAMD 2.12 [33] package to investigate the capability of zeolite membranes for water permeability and heavy metal rejection. Furthermore, VMD 1.9.3 [34] was used for visualization and analysis of the atomistic results.

External pressures from 10 to 200 MPa were applied to the system to consider the behavior of the system at each pressure. To apply external pressure, the external constant force (f in pN) which is known as pressure-driven flow [35], was applied to the system to induce pressure difference (ΔP in Pa) between two sides of the membrane,

$$\Delta P = \frac{f \cdot n}{A} \quad (1)$$

where A is the area of membrane ($A = 1.44 \times 10^{-17} \text{ m}^2$) and n is the number of water molecules. $F = \frac{\Delta p \cdot A}{n}$. This technique has been used in many previous works [36–38]. For each selected applied pressure, 4–6 independent MD simulations with uncorrelated initial configurations were performed.

The following steps were followed to perform the MD simulations. First, the energy of the system was minimized during 100,000 steps at zero-temperature. Then, it was equilibrated at pressure of 10^5 Pa and temperature of 298 K for 1 ns. The temperature of the system was kept constant at 298 K by Langevin thermostat with a time constant of 0.1 ps. It is known that the water diffusion will not be affected significantly by this thermostat. [39] To further equilibrate, MD simulations were performed in the canonical ensemble (NVT) for 1 ns. Finally, the simulations were carried out for 10 ns in various applied pressures from 10 to 200 MPa.

The silicon and oxygen atoms of zeolite were assumed to be rigid for avoiding the vertical displacement of the membranes. However, the structure of the bulk zeolite might slightly vary while loaded with water molecules [40], because OH groups on the surface of the zeolite were flexible. It has already been shown that the structural flexibility effect on the separation performance of zeolites was negligible [12,41] and it is anticipated that the outcomes of our study are not significantly affected by assuming a rigid structure. The cutoff radius of 12.0 \AA and the Particle Mesh Ewald [42] were used for short-range interactions and long-range interactions, respectively. In addition, the Lorentz-Berthelot mixing rules [43] were used for nonbonded interaction of LJ parameters between dissimilar atoms as used in previous works [12,41].

During the simulation, the position of heavy metal ions and water

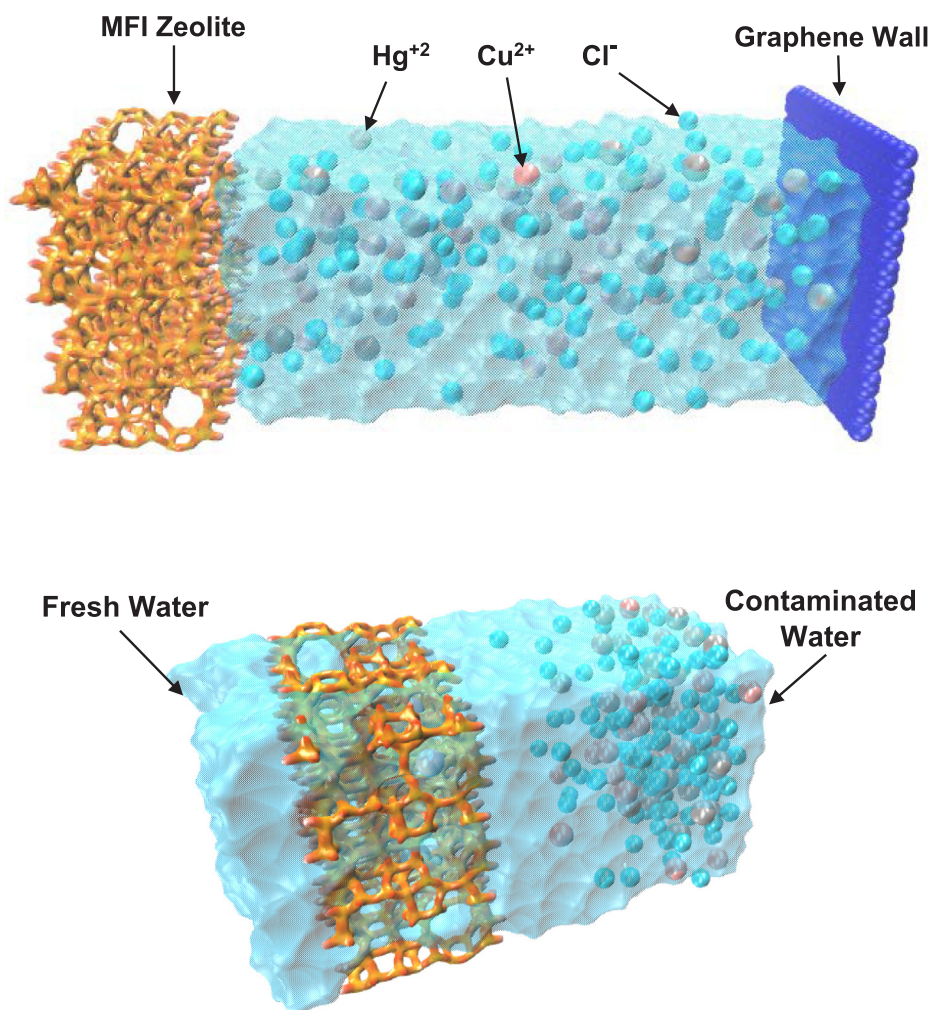


Fig. 1. Top: Schematic of the problem before ion separation at 50 MPa; bottom: Ion separation at 50 MPa after 10 ns MD simulation.

molecules were monitored to calculate the ion rejection and the water permeability of the considered zeolite nanosheet. Water molecules permeate through the membrane and accumulate on the permeate side of the simulation box, so that water flux could be calculated from the slope of a number of permeated water molecules. Fig. 1 shows the schematic of the problem before and after separation at an arbitrary applied pressure of 50 MPa.

Diffusion coefficient of water molecules in solution from a MD simulation using Eq. (2), was calculated to validate the result with the literature.

$$D = \frac{1}{2n} \cdot \frac{\langle |\bar{r}_{(t+t_0)} - \bar{r}_{(t_0)}|^2 \rangle}{t} \quad (2)$$

where D is the diffusion coefficient, n is the dimensionality of the system, t is time, $\bar{r}_{(t+t_0)}$ is the position of the ion at the time $(t + t_0)$ and $\bar{r}_{(t_0)}$ is the initial position. As the MD simulations were performed in three-dimensions, then $n = 3$. The numerator of Eq. (2) is the mean square displacement (MSD). By saving the positions as a function of time, we can calculate the MSD and then obtain a diffusion coefficient. We performed independent MD sampling runs using the same starting coordinates, and then the mean MSD was calculated by running average of MSD of trajectories. The finally least-squares fitting was applied to estimate the slope of MSD versus simulation time, and the diffusion coefficient was one-sixth of the slope. The diffusion coefficients for water molecules in this work using an NVT ensemble was obtained as $2.34 \times 10^{-9} \text{ m}^2 \text{ s}^{-1}$. This MD result is in good agreement with that of

Han et al. [39] which is $2.1 \times 10^{-9} \text{ m}^2 \text{ s}^{-1}$, that implies 11.42% maximum error. This parameter also showed that the TIP3P model is a robust model for the current simulations.

For further validation, the water permeability of the system was calculated and validated against experimental data of Liu et al. [41]. Water permeability is the liter of the permeated water molecules per 1 h through the nanoporous membrane with 1 m^2 area by applying the pressure of 1 bar. Hence, it should be calculated to compare the performance of membranes. The water permeability of the system was obtained as $763 \text{ L/m}^2 \text{ h bar}$ ($2.119 \times 10^{-9} \text{ m Pa}^{-1} \text{ s}^{-1}$). This water permeability is comparable with $\sim 2 \times 10^{-9} \text{ m Pa}^{-1} \text{ s}^{-1}$ in the literature with $\sim 5.9\%$ maximum error for the water desalination using zeolite membranes [41].

3. Results and discussions

Results of NAMD simulations after 10 ns at different applied pressures were shown in Table 1 in terms of number of permeated ions through the MFI membrane. It can be seen from the table that at any applied pressure to the system, the Zeolite membrane does not allow the copper and mercury to permeate. The membrane also keeps all chlorine behind the membrane at pressures 10 to 75 MPa while few ions could pass at 100 and 200 MPa. This turns out 100% ion rejection at all studied applied pressures for copper and mercury. The permeation of a few chlorine ions at high applied pressures can be due to overcoming the van der Waals and electrostatic interactions between the ions and

Table 1
Number of permeated ions after 10 ns through the membrane.

Ions	Applied pressure (MPa)								
	10	20	30	40	50	75	100	150	200
Cu ²⁺	0	0	0	0	0	0	0	0	0
Hg ²⁺	0	0	0	0	0	0	0	0	0
Cl ⁻	0	0	0	0	0	0	3	6	9

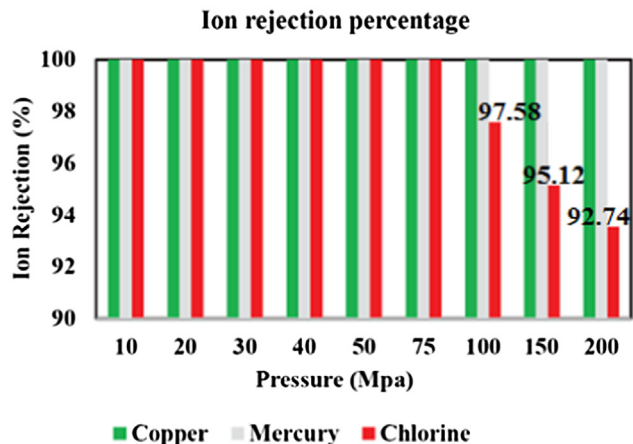


Fig. 2. Ion rejection versus pressure using Zeolite MFI nanosheet.

the membrane.

As shown in Fig. 2 100% chlorine ions rejection happened from 10 to 75 MPa and 97.58%, 95.12 and 92.74% at pressures 100, 150 and 200 MPa, respectively.

This process can be seen in Fig. 3 as well. It is clear from the figure that at P = 50 MPa after 10 ns, only fresh water permeates through the membrane but at P = 100 MPa other than water, three ions of chlorine can pass along with pure water. A high and desirable percentage of ion

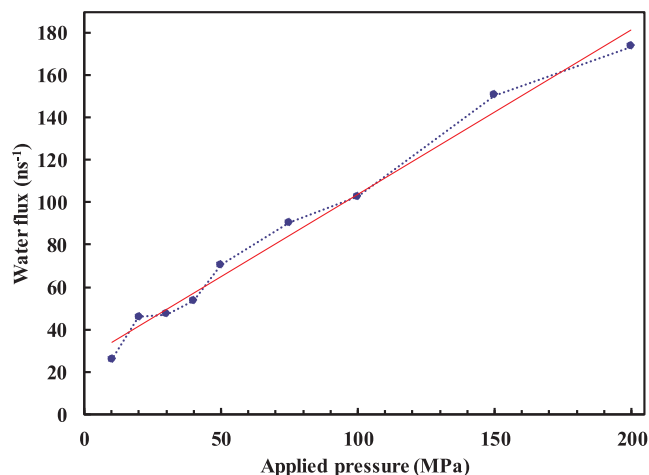


Fig. 4. Water flux versus pressure.

is separated out of contaminated water and it is so promising.

One of the main advantages of the recommended membrane, other than perfect ion rejection, is its high-water flux property that distinguishes it from other nanosheet membranes. The water flux J is the number of permeated water molecules per nanosecond [9] and it is obtained by the Hagen-Poiseuille's law: [44,45]

$$J = \frac{\Delta P \epsilon r^2}{8 \eta l} \tag{3}$$

where ϵ is the membrane porosity, r is the pore radius, η is the viscosity and l is the membrane thickness. According to Fig. 4, water flux during the separation process increased from 25.6 ns^{-1} at 10 MPa to 173.6 ns^{-1} at 200 MPa. As seen in the figure, the water flux increases linearly by increasing pressure. This amount of water flux is so promising and can lead to reductions in the costs and energy in future

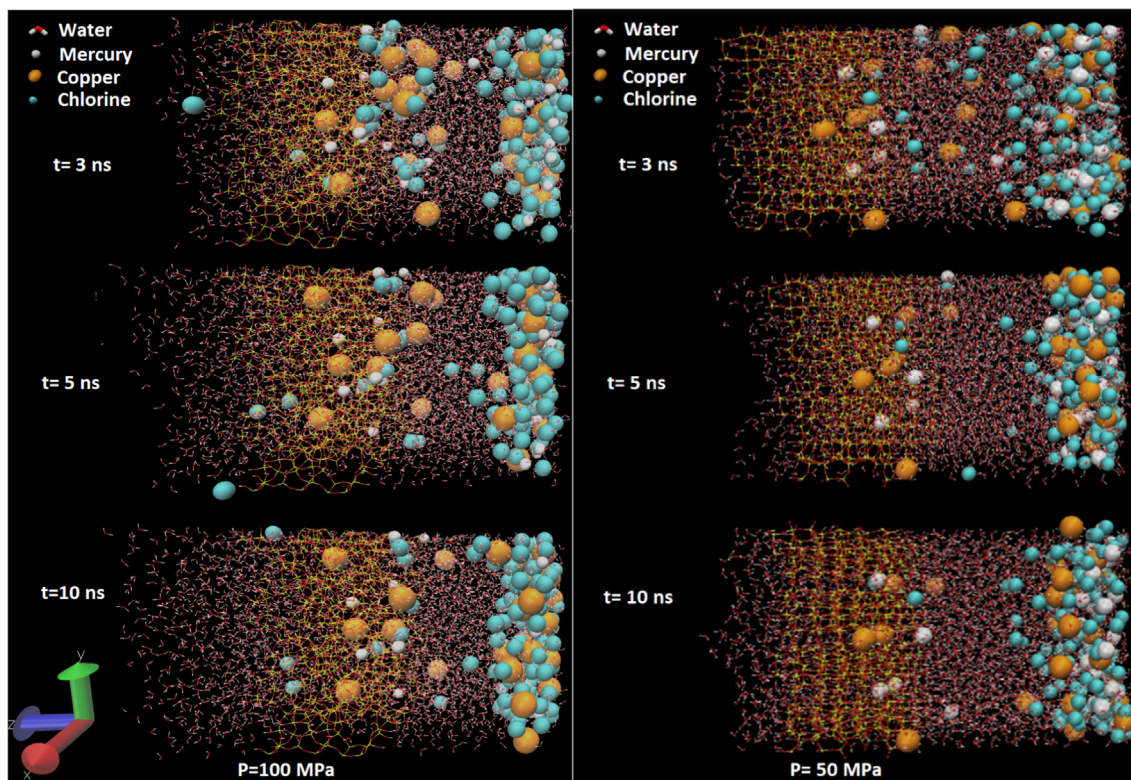


Fig. 3. Separation process at different times and pressures using MFI zeolite.

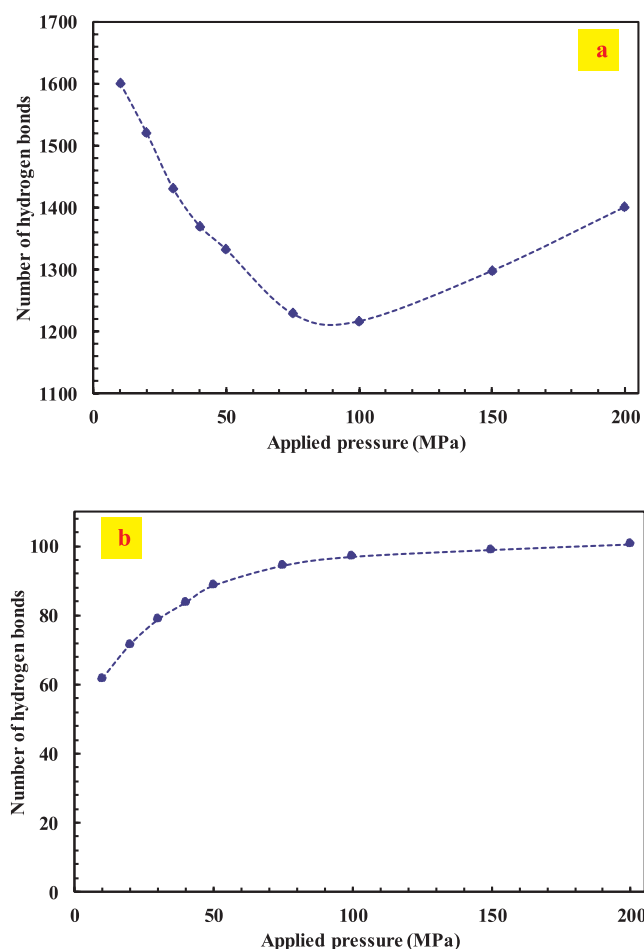


Fig. 5. Number of hydrogen bonds between water molecules versus pressure (a): The whole simulation box; (b): inside membrane.

designs [46].

Fig. 5(a) shows the number of hydrogen bonds at different pressures throughout the system. As can be seen, the number of hydrogen bonds decrease due to change in water molecule structure and their collision with the membrane. By increasing the applied pressure, the water flux through the membrane also increases. Then, water molecules move faster, and the particles spread out in all directions and collide more with each other and the membrane. As the water molecules slide past each other, hydrogen bonds are constantly formed and broken. Due to higher kinetics of the molecules in higher applied pressures, the breaking of these bonds is caused more by the motion of the water molecules due to the heat arise by friction of molecules for permeating through the membrane. As the water molecules approach the surface of the zeolite sheet, the number of hydrogen bonds vary along the un-uniformed structure of the zeolite matrix. Therefore, an unexpected increase in hydrogen bond can be seen from 100 to 200 MPa. As shown in Fig. 5a, the number of hydrogen bonds decrease throughout the whole system until 100 MPa and then shows an uptrend in higher applied pressures. From low pressures up to 100 MPa, more water molecules accumulate inside the membrane that causes reduction of hydrogen bonds in the whole system. At the same time, fresh water flux is not that much to compensate decrease of hydrogen bonds due to entering of water molecules in to the membrane. However, when applied pressures is higher than 100 MPa, the fresh water flux increases gradually and number of water molecules that are leaving the membrane to permeate to the other side upsurge.

This phenomenon compensates the reduction trend in number of hydrogen bonds and shifts it from a decreasing to an uptrend. The other

reason can be existence of impurities after separation in water. The presence of few chlorin ions in the water that have permeated in ≥ 100 MPa, can delay the water phase change and that will increase the number of hydrogen bond formation by water molecules as there is not enough energy to break the bonds. The presence of the large number of water molecules alongside the pore edges at 200 MPa could also be a reason for an insignificant change in hydrogen bonds number with respect to its value at some low pressures. Hydrogen bonds form between water molecules at the beginning of the simulations when no molecules permeated through the membrane. Once the pressure is applied, water molecules enter inside the membrane and move to the other side of the nanosheet. During the presence of water molecules inside the membrane, number of hydrogen bonds decrease significantly since there is not enough room for the molecules inside the membrane due to limited space inside it as demonstrated in Fig. 5b. At high applied pressure greater than 75 MPa, the number of hydrogen bonds inside the membrane is not changing too much because of the membrane saturation.

To depict how density changes as a function of distance from a reference ion, the radial distribution function (RDF), or pair correlation function $g(r)$, has been computed for both water-copper and water-mercury in Fig. 6 at 50 MPa. The $g(r)$ gives the probability of finding a molecule in the distance r from another molecule that has been separated by different distances r at different times by Brownian motion. As seen, because of the strong repulsive forces at short distances (less than atomic diameter), $g(r)$ is zero. Based on the results, the RDF first and large peak occurs around 1.8 Å and 2.15 Å for water-copper and water-mercury, respectively. These peaks of $g(r)$ having a value of about 16 and 18 for the two $\text{Cu}^{2+}-\text{H}_2\text{O}$ and $\text{Hg}^{2+}-\text{H}_2\text{O}$, respectively. This means that it is 16 and 18 times more likely that two molecules would be found at this separation.

Also, there is not a sensible change in that aggregation at different applied pressures for water-copper and water-mercury. The RDF then falls and passes through a minimum value around $r = 3.2$ Å. The chances of finding two atoms with this separation are less. At long distances, $g(r)$ approaches to three which indicates there is no long-rang order. Furthermore, integration of RDF was computed and shown in the figure which resembles hydration number of a molecule: [47]

$$n(r) = 4\pi\rho \int_0^r g(r) r^2 dr \quad (4)$$

where $n(r)$, ρ and r are the hydration number, density and the radial coordinate, respectively. The value of integration of RDF decreases by increasing the applied pressure.

To show the distribution of water in different areas before and after the membrane, water density maps at various applied pressures were plotted in Fig. 7 using VolMap plugin in VMD. As shown, water density gently increases in the left side of the membrane. As seen in the figure,

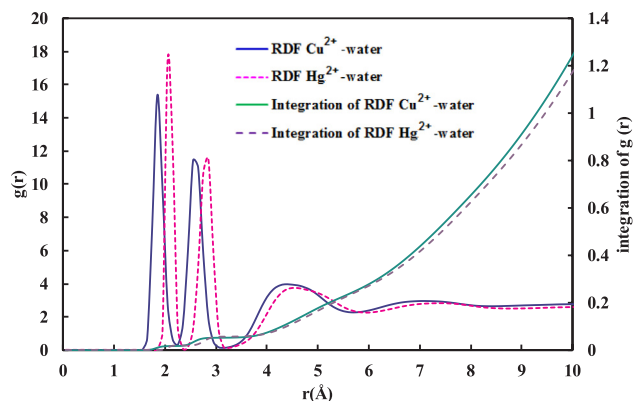


Fig. 6. RDF and integration of RDF for copper-water and mercury-water in simulation box at an arbitrary applied pressure of 50 MPa.

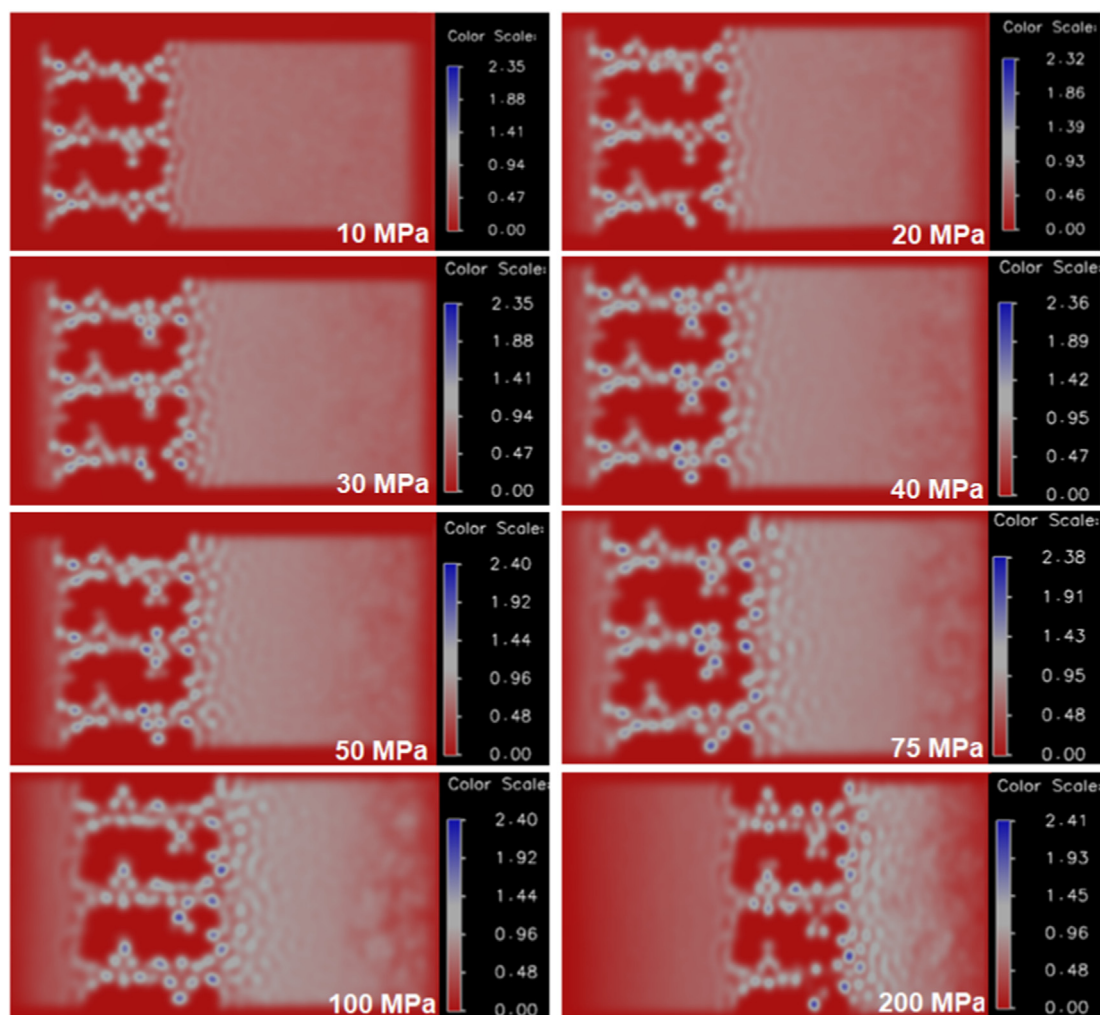


Fig. 7. Water density map of the system at various applied pressures.

the water density at 10 MPa is higher in the right side because not many water molecules permeated through the membrane. While at 200 MPa with more fresh water flux, the water molecules accumulation is seen in the left side. According to the water density contours, water molecules passes from some specific paths which have enough space for the molecules to commute.

Fig. 8 depicts these trends and shows water density distribution in three main regions before permeation, inside the membrane and after passing from the membrane. Water density (accumulation of water molecules) peak increases with pressure and shifts toward the left side which turns into more fresh water. It is clear that when the force behind the water molecules pushes them toward the membrane, the water molecules accumulation increases near the membrane and subsequently, the density increases due to resistance against ion permeation through the membrane and decreases again inside the membrane because of few ions which permeated in. In some applied pressures (10, 30, 100 and 200 MPa) the density profile of water molecules presented in Fig. 8 to study the water structure inside the simulation box for specifying the arrangements of water molecules in different sections. As shown in the figure, arrangements of water molecules were not same in all locations and they accumulated close to the membrane due to the non-bonded van der Waals interaction of water molecules and membrane atoms.

According to the results presented in this work, it is apparent that ions could not pass from the membrane in low pressures. Therefore, one random ion was picked from each type to show their tracking path in

Fig. 9a. Dashed lines show the membrane position at the middle of the simulation box. As seen, in a low pressure such as 10 MPa, not only no ion could penetrate through the membrane but also, they have not even entered to the zeolite and continued their movement within the solvent.

This is different at higher pressures like 200 MPa. The ions are able to penetrate inside the membrane due to presence of enough force for their transportation in terms of applied pressure. Few chlorine ions passed through the membrane as seen in Table 1 but other positive charged ions were trapped inside the membrane. Such a result was shown in Fig. 9b that exemplifies that 200 MPa was not enough to pass ions from the membrane pores and zeolite MFI nanomembrane is a great candidate for separation of these ions out of water even at high pressures which are closer to the real-world applications. Per Fig. 9b, the ion tracking path was shown for one of those nine chlorine ions that could leave the membrane, and one of those that was trapped inside the membrane.

The Fig. 10 shows Van der Waals interactions of water-membrane is much stronger than the ions-membrane. This leads the water molecules to penetrate inside the zeolite MFI nanomembrane without any applied pressure but it is vice versa for the ions and they need to be forced for penetration. On the other hand, after applying the pressure to the system, not only the water molecules can penetrate into the membrane faster, but also they exit from the membrane easier while this applied pressure can only pushes the ions to the zeolite.

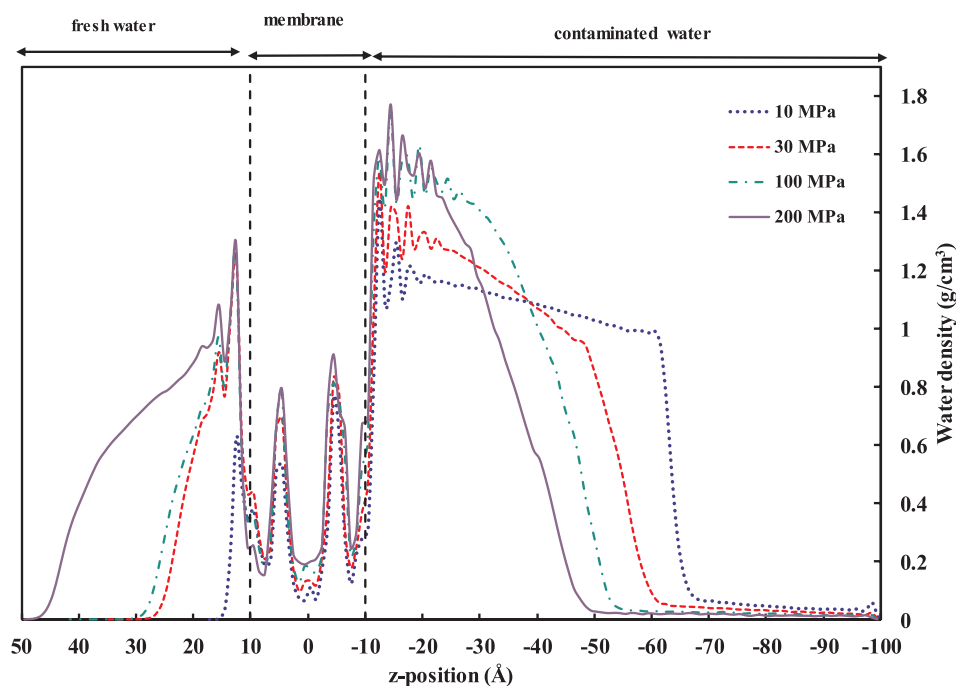


Fig. 8. Density profile of water molecules at various applied pressures.

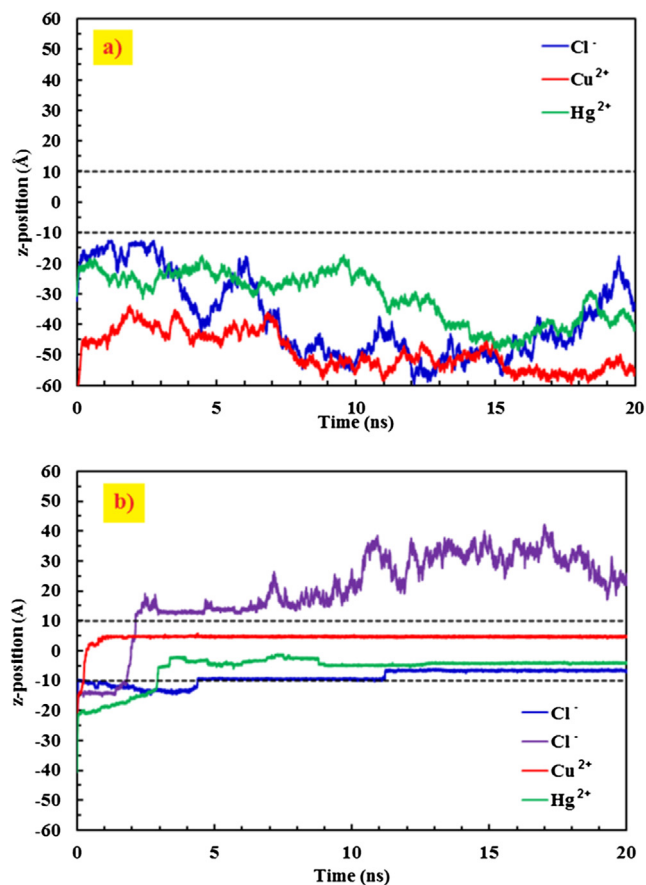


Fig. 9. Ions tracking path at (a) 10 and (b) 200 MPa for randomly selected ions.

4. Conclusions

By means of non-equilibrium MD simulations, it was shown that how zeolite MFI membrane can be highly efficient for water

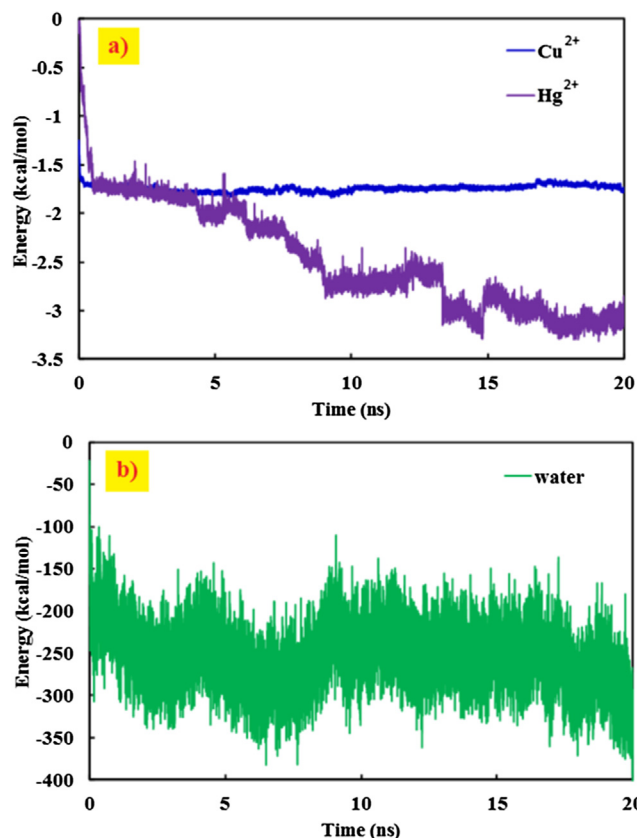


Fig. 10. Van der Waals interactions of (a) ions and (b) water molecules with the nanomembrane.

purification. The two hazardous chemicals, the copper chloride and mercury chloride, were added to water in the simulation box. Various pressures were applied to the system for investigating the separation process in a reverse osmosis system, from 10 MPa to 200 MPa. In all applied pressures to the system, the zeolite membrane rejected 100% of

the copper and mercury ions from water with a high chlorine ions rejection of 97.6% at 100 MPa and 93.6% at 200 MPa and 100% at other lower applied pressures. Simultaneous high-water flux and ion rejection, as an important factor in membrane technology, was seen in the implemented zeolite. These behaviors of the zeolite MFI make it a competitive candidate for fast and efficient water purification. Furthermore, with improvement of industrial fabrication technology, it could be produced to be stable and large enough for realistic applications as an earth-abundant and cost-effective material.

Declaration of Competing Interest

We would like to confirm that there is no known conflict of interest associated with this publication.

References

- <https://nj.gov/health/eoh/rtkweb/documents/fs/0532.pdf>.
- <http://www.labchem.com/tools/msds/msds/LC16590.pdf>.
- M.A. Shannon, P.W. Bohn, M. Elimelech, J.G. Georgiadis, B.J. Mariñas, A.M. Mayes, Science and technology for water purification in the coming decades, *Nature* 452 (2008) 301.
- M.M. Pendergast, E.M.V. Hoek, A review of water treatment membrane nano-technologies, *Energy Environ. Sci.* 4 (2011) 1946–1971.
- K.S. Spiegler, Y.M. El-Sayed, The energetics of desalination processes, *Desalination* 134 (2001) 109–128.
- K.M. Gupta, Z. Qiao, K. Zhang, J. Jiang, Seawater pervaporation through zeolitic imidazolate framework membranes: atomistic simulation study, *ACS Appl. Mater. Interf.* 8 (2016) 13392–13399.
- D. Cohen-Tanugi, J.C. Grossman, Water desalination across nanoporous graphene, *Nano Lett.* 12 (2012) 3602–3608.
- M. Hosseini, J. Azamat, H. Erfan-Niya, Improving the performance of water desalination through ultra-permeable functionalized nanoporous graphene oxide membrane, *Appl. Surf. Sci.* 427 (2018) 1000–1008.
- M. Heiranian, A.B. Farimani, N.R. Aluru, Water desalination with a single-layer MoS₂ nanopore, *Nat. Commun.* 6 (2015) 8616.
- H. Gao, Q. Shi, D. Rao, Y. Zhang, J. Su, Y. Liu, Y. Wang, K. Deng, R. Lu, Rational design and strain engineering of nanoporous boron nitride nanosheet membranes for water desalination, *J. Phys. Chem. C* 121 (2017) 22105–22113.
- A. Khataee, G. Bayat, J. Azamat, Molecular dynamics simulation of salt rejection through silicon carbide nanotubes as a nanostructure membrane, *J. Mol. Graph. Model.* 71 (2017) 176–183.
- S.H. Jamali, T.J.H. Vlugt, L.-C. Lin, Atomistic understanding of zeolite nanosheets for water desalination, *J. Phys. Chem. C* 121 (2017) 11273–11280.
- J. Azamat, A. Khataee, S.W. Joo, Functionalized graphene as a nanostructured membrane for removal of copper and mercury from aqueous solution: a molecular dynamics simulation study, *J. Mol. Graph. Model.* 53 (2014) 112–117.
- J. Azamat, A. Khataee, S.W. Joo, Molecular dynamics simulation of trihalomethanes separation from water by functionalized nanoporous graphene under induced pressure, *Chem. Eng. Sci.* 127 (2015) 285–292.
- P. Ansari, J. Azamat, A. Khataee, Separation of perchlorates from aqueous solution using functionalized graphene oxide nanosheets: a computational study, *J. Mater. Sci.* 54 (2019) 2289–2299.
- J. Azamat, B.S. Sattary, A. Khataee, S.W. Joo, Removal of a hazardous heavy metal from aqueous solution using functionalized graphene and boron nitride nanosheets: Insights from simulations, *J. Mol. Graph. Model.* 61 (2015) 13–20.
- J. Azamat, A. Khataee, F. Sadikoglu, Separation of carbon dioxide and nitrogen gases through modified boron nitride nanosheets as a membrane: insights from molecular dynamics simulations, *RSC Adv.* 6 (2016) 94911–94920.
- J. Azamat, A. Khataee, Improving the performance of heavy metal separation from water using MoS₂ membrane: Molecular dynamics simulation, *Comput. Mater. Sci.* 137 (2017) 201–207.
- J. Azamat, A. Khataee, F. Sadikoglu, Computational study on the efficiency of MoS₂ membrane for removing arsenic from contaminated water, *J. Mol. Liq.* 249 (2018) 110–116.
- S. Homaieghar, M. Elbahri, Graphene membranes for water desalination, *NPG Asia Mater.* 9 (2017) e427.
- W.J. Roth, J. Čejka, Two-dimensional zeolites: dream or reality? *Catal. Sci. Technol.* 1 (2011) 43–53.
- R. Wei, H. Yang, J.A. Scott, K.-F. Aguey-Zinsou, D. Zhang, Synthesis of 2D MFI zeolites in the form of self-interlocked nanosheet stacks with tuneable structural and chemical properties for catalysis, *Appl. Mater. Today* 11 (2018) 22–33.
- K. Na, C. Jo, J. Kim, K. Cho, J. Jung, Y. Seo, R.J. Messinger, B.F. Chmelka, R. Ryoo, Directing zeolite structures into hierarchically nanoporous architectures, *Science* 333 (2011) 328.
- K.Y. Foo, B.H. Hameed, The environmental applications of activated carbon/zeolite composite materials, *Adv. Colloid Interf. Sci.* 162 (2011) 22–28.
- D. Pacilé, J.C. Meyer, A. Fraile Rodríguez, M. Papagno, C. Gómez-Navarro, R.S. Sundaram, M. Burghard, K. Kern, C. Carbone, U. Kaiser, Electronic properties and atomic structure of graphene oxide membranes, *Carbon* 49 (2011) 966–972.
- J. Azamat, A. Khataee, S.W. Joo, Separation of copper and mercury as heavy metals from aqueous solution using functionalized boron nitride nanosheets: A theoretical study, *J. Mol. Struct.* 1108 (2016) 144–149.
- F.S. Emami, V. Puddu, R.J. Berry, V. Varshney, S.V. Patwardhan, C.C. Perry, H. Heinz, Force field and a surface model database for silica to simulate interfacial properties in atomic resolution, *Chem. Mater.* 26 (2014) 2647–2658.
- E.R. Cruz-Chu, A. Aksimentiev, K. Schulten, Water – silica force field for simulating nanodevices, *J. Phys. Chem. B* 110 (2006) 21497–21508.
- P.E.M. Lopes, V. Murashov, M. Tazi, E. Demchuk, A.D. MacKerell, Development of an empirical force field for silica. Application to the quartz – water interface, *J. Phys. Chem. B* 110 (2006) 2782–2792.
- W.L. Jorgensen, J. Chandrasekhar, J.D. Madura, R.W. Impey, M.L. Klein, Comparison of simple potential functions for simulating liquid water, *J. Chem. Phys.* 79 (1983) 926–935.
- X. Meng, J. Huang, Enhancement of water flow across a carbon nanotube, *Mol. Simul.* 42 (2016) 215–219.
- M. Thomas, B. Corry, A computational assessment of the permeability and salt rejection of carbon nanotube membranes and their application to water desalination, *Philos. Trans. R. Soc. London, Ser. A* 374 (2016).
- J.C. Phillips, R. Braun, W. Wang, J. Gumbart, E. Tajkhorshid, E. Villa, C. Chipot, R.D. Skeel, L. Kale, K. Schulten, Scalable molecular dynamics with NAMD, *J. Comput. Chem.* 26 (2005) 1781–1802.
- W. Humphrey, A. Dalke, K. Schulten, VMD: visual molecular dynamics, *J. Mol. Graph.* 14 (1996) 33–38.
- F. Zhu, E. Tajkhorshid, K. Schulten, Theory and simulation of water permeation in aquaporin-1, *Biophys. J.* 86 (2004) 50–57.
- J. Goldsmith, C.C. Martens, Pressure-induced water flow through model nanopores, *PCCP* 11 (2009) 528–533.
- W.-F. Chan, H.-Y. Chen, A. Surapathi, M.G. Taylor, X. Shao, E. Marand, J.K. Johnson, Zwitterion functionalized carbon nanotube/polyamide nocomposite membranes for water desalination, *ACS Nano* 7 (2013) 5308–5319.
- B. Corry, Designing carbon nanotube membranes for efficient water desalination, *J. Phys. Chem. B* 112 (2008) 1427–1434.
- K.N. Han, S. Bernardi, L. Wang, D.J. Searles, Water diffusion in zeolite membranes: molecular dynamics studies on effects of water loading and thermostat, *J. Membr. Sci.* 495 (2015) 322–333.
- A. Sartbaeva, S.A. Wells, M.M.J. Treacy, M.F. Thorpe, The flexibility window in zeolites, *Nat. Mater.* 5 (2006) 962–965.
- Y. Liu, X. Chen, High permeability and salt rejection reverse osmosis by a zeolite nano-membrane, *PCCP* 15 (2013) 6817–6824.
- T. Darden, D. York, L. Pedersen, Particle mesh ewald: an N-log(N) method for ewald sums in large systems, *J. Chem. Phys.* 98 (1993) 10089–10092.
- L. Viola, S. Lloyd, Dynamical suppression of decoherence in two-state quantum systems, *Phys. Rev. A* 58 (1998) 2733–2744.
- R.W. Baker, *Membrane technology and applications*, Wiley, 2012.
- J.R. Werber, C.O. Osuji, M. Elimelech, Materials for next-generation desalination and water purification membranes, *Nat. Rev. Mater.* 1 (2016) 16018.
- D. Cohen-Tanugi, R.K. McGovern, S.H. Dave, J.H. Lienhard, J.C. Grossman, Quantifying the potential of ultra-permeable membranes for water desalination, *Energy Environ. Sci.* 7 (2014) 1134–1141.
- M. Duan, X. Song, S. Zhao, S. Fang, F. Wang, C. Zhong, Z. Luo, Layer-by-layer assembled film of asphaltene/polyacrylamide and its stability of water-in-oil emulsions: a combined experimental and simulation study, *J. Phys. Chem. C* 121 (2017) 4332–4342.